POTENTIAL OF UNCONVENTIONAL LOW-NOISE PROPULSION DESIGNS FOR UAV/UAM APPLICATIONS

Adam Sieradzki, Lukasiewicz Research Network, Institute of Aviation, Warsaw, Poland
Pawel Kekus-Kumor, Lukasiewicz Research Network, Institute of Aviation, Warsaw, Poland
Witold Klimczyk, Lukasiewicz Research Network, Institute of Aviation, Warsaw, Poland

Abstract

The aim of this work is to evaluate the potential of unconventional low-noise propulsion designs for UAV and UAM vehicles. The paper presents three types of proposed solutions for reducing noise and improving propulsion system performance. The first proposal addresses the issue of increased noise due to the interaction between propellers and supporting arms, exploring noise mitigation possibilities through a novel arm design. The subsequent two proposals involve coaxial co-rotating rotors and ducted rotors with compact duct design, which aim to improve aeroacoustic performance while maintaining the same propulsor diameter as the reference isolated propeller. The paper presents the results of experimental tests of the prototype solutions conducted in an anechoic chamber in hover conditions. Comparisons with the reference case demonstrated significant potential of the proposed solutions, allowing to achieve noise reduction of up to 17.2 dB(A) and aerodynamic efficiency improvement of up to 5%.

1. NOTATION

Symbols:

C_T	Thrust coefficient, $T/(\rho_\infty \pi \Omega^2 R^4)$
C_Q	Torque coefficient, $Q/(\rho_\infty \pi \Omega^2 R^5)$
d	Axial separation (stacked rotors), mm
FM	Figure of Merit, $C_T^{1.5}/\left(C_Q\sqrt{2}\right)$
P	Power, W
R	Rotor radius, outer duct radius, m
T, T_D	Overall thrust, duct thrust, N
Q	Torque, Nm
θ	Polar angle of microphone, deg
ρ_∞	Freestream density, kg/m^3
φ	Azimuthal sep. (stacked rotors), deg
Ψ	Azimuthal angle of microphone, deg
Ω	Propeller speed of rotation, rad/s

Acronyms:

BPF	Blade Passing Frequency
PSD	Power Spectral Density
RANS	Reynolds-Averaged Navier-Stokes
SPL	Sound Pressure Level
UAM	Urban Air Mobility
UAV	Unmanned Aerial Vehicle

2. INTRODUCTION

The market for Unmanned Aerial Vehicles (UAV) and Urban Air Mobility (UAM) vehicles is currently a rapidly growing sector of the industry. However, there are several factors that could potentially limit the development in this field. One of the commonly mentioned challenges associated with UAV/UAM vehicles is the issue of noise emitted by them (Ref. 1). Due to the negative impact of noise on the well-being and health of people (Ref. 2), there are plans to introduce a series of regulations in the near future to limit the acoustic power generated by these aircraft.

Therefore, there is a clear need for the development of low-noise propulsion technologies for use in UAV/UAM vehicles. The most fundamental and annoying source of noise in this case are the rotors (Ref. 3), which can serve both lifting and propelling function. To achieve an aircraft with low noise emissions, most attention is focused on the proper design (optimization) of rotor geometry, taking into account aeroacoustic criteria. Typically, this type of design is carried out for isolated rotors, as it significantly simplifies the computational methodology (Ref. 4-7). However, UAV/UAM vehicles are characterized by diverse configurations, and their rotors usually operate in close proximity to other structural elements, e.g. arms serving as the mounting point for electric motors. The aerodynamic interactions in this case can significantly affect the level of emitted noise (Ref. 8).

Operations performed by UAV/UAM vehicles are largerly carried out in urban environments, requiring vertical takeoff and landing (VTOL) capabilities. Simultaneously, due to factors such as limited landing space, there is a search for propulsion systems characterized by high lift capacity with small dimensions. For this reason, ducted rotors are often used in these aircraft, which additionally have a positive impact on the safety of operators and personnel. Another example of a solution that increases the thrust of a propulsion system while maintaining similar dimensions are coaxial rotors.

This paper focuses on assessment of the potential of selected technical solutions, which address the aforementioned problems and challenges currently faced by the UAV/UAM industry. The evaluation takes into account both acoustic aspects and those related to aerodynamic performance. Regarding the interaction of rotors with aircraft structure, the interaction of the rotor wake with arms of different shapes was analyzed. The second examined case was the ducted propulsion system, characterized by a compact duct design (low chord-to-diameter ratio) compared to most solutions discussed in the literature (Ref. 9-12), and thus, with high applicative value for small unmanned aerial vehicles. The third solution subjected to analysis was coaxial rotors. While contra-rotating coaxial rotors are a common configuration in UAVs, this study focused on co-rotating rotors (known as stacked rotors) due to their significantly lower acoustic emission. This paper presents general conclusions drawn from the comparison of the abovementioned UAV/UAM aircraft propulsion configurations.

3. METHODOLOGY

The assessment of the potential of selected technical solutions was conducted primarily through experimental research in a newly constructed acoustic chamber at the Lukasiewicz – Institute of Aviation (ILOT). A single, commercially available, two-blade propeller, the APC 12x5.5 MR, was selected as a reference case for acoustic and performance comparisons. A CAD model of the basic propeller was created based on tabular data obtained from the APC Propellers website and a 3D scan of the propeller geometry. Mutual comparison of the analyzed cases was possible due to the consistency of parameters such as propulsor dimensions (maintaining the same maximum diameter) and the range of generated thrust.

Various computational methods were utilized in preparation for this study to obtain prototype geometries, ranging from simple codes for designing and analyzing ducted propulsion systems using lifting line theory and the panel method, to advanced unsteady simulations using a Navier-Stokes solver. However, in this paper, the greatest emphasis is placed on the discussion of experimental research.

3.1. Anechoic chamber

The anechoic chamber at the ILOT is in the form of a freestanding room constructed within an existing hall using a semi-custom drywall system, which rests on an array of mechanical vibration isolators. Internally, the chamber is 4.40 m deep, 4.15 m wide, and 5.00 m high. In order to ensure anechoic conditions within the room, the entire surfaces of the walls, the roof and the floor were covered with foam wedges, with corners filled with appropriate rectangular blocks, leaving no hard surface exposed. The wedges have a total height of 500 mm and a base of 300 mm × 300 mm with a thickness of 100 mm. The tip-to-tip dimensions of the chamber are 3.40 m × 3.15 m × 4.00 m. The designed cut-off frequency of the chamber is 170 Hz. The background noise inside the chamber does not exceed 18 dB(A).

3.2. Test rig

In this study three configurations of a testing rig were used, allowing for testing of three different types of interactions. Testing of stacked rotors required the simplest baseline configuration of the test stand, consisting only of the main drive and measurement head. A dedicated long shaft was used to get axial separation of rotors up to 60 mm (20% diameter), as shown in Figure 1. All necessary components of the measurement head were designed to fit in a theoretical tube with a diameter of 50 mm, to minimize the impact of the test stand on the aeroacoustic performance of propellers. The propeller axis is positioned vertically to guide the propeller wake along the longest dimension of the chamber. The length of the tube is configured so that the propellers are situated approximately 1.3 m above the tips of the floor wedges. Propellers are tested in an inverted orientation. As a result, the propellers generate downward thrust while directing airflow upwards.

Figure 1: Test rig configuration for testing stacked rotors

Embedded within the main test rig head are an AXI 2814/28 V2 BLDC electric motor with a RiKO PRC-320 optical revolution sensor, a FUTEK QTA143 torque meter, and an Octogon FSA-50 thrust meter. The motor is mounted directly to the torque meter, but due to the thrust sensor's fragility (a single M3 interface on both sides), linear bearings were located between the two sensors. These remove lateral loads from the thrust meter. The high quality of results obtained with the baseline test rig configuration inside the ILOT anechoic chamber was confirmed by benchmark testing, as presented in Ref. 13-14.

For the two other interaction types, the rig was expanded with a frame supporting elements imitating the structure of the airframe – arms and ducts. The arms were mounted on a freestanding single cantilever through a KD45 (+/- 5 N) bending beam force sensor, but data acquired by this sensor was not analyzed in the presented study. In contrast, the testing of ducted rotors required a much more rigid and secure setup to precisely fix the duct's position relative to the propeller axis and to maintain circumferentially constant blade tip clearance (about 0.8 mm for the analyzed cases). To measure the thrust generated by the ducts, two KD45 (+/- 10 N) bending beam force sensors were used. The two setups are presented in Figure 2 and Figure 3. As shown in the pictures, all structural elements of the stands were covered with foam to reduce acoustic reflections.

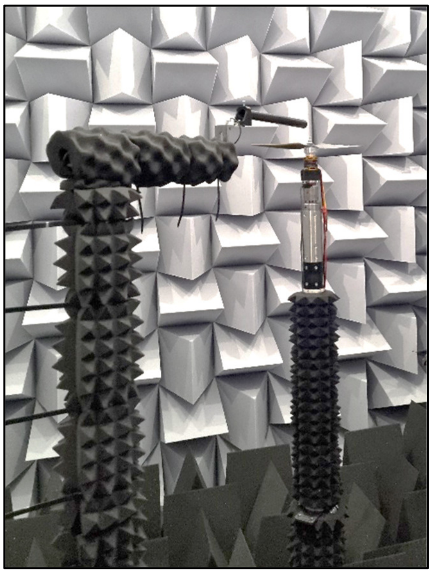

Figure 2: Test rig configuration for testing the rotor-arm interaction

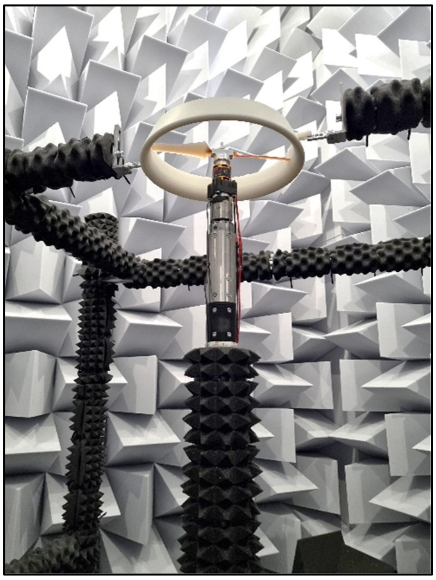

Figure 3: Test rig configuration for testing ducted rotors

3.3. Data acquisition

All acoustic measurements were performed using PCB 378B02 free-field microphones. The data acquisition system consisted of two NI cDAQ-9189 chassis with NI-9250 cards for the microphones, as well as NI-9203 and NI-9205 cards for load, RPM and atmospheric sensors. Microphone signals were acquired at 51.2 kHz. Thrust and torque, as well as RPM and the atmospheric parameters, were acquired at 10 kHz. The signals were sampled for 5 s, shortly after the propeller reached the desired rotational speed, to avoid recirculation effects, as discussed in Ref. 15. In this specific experimental configuration, these effects typically begin to manifest approximately 10 seconds after the propeller starts spinning.

The acquired acoustic signals were split into Hanning-windowed Welsh blocks for the calculation of the power spectral density (PSD) of acoustic pressure, with a reference pressure of 20 μPa and A-weighting used for all measurements. All sound pressure level (SPL) values were calculated by integrating the spectra of acoustic pressure between 100 Hz and 20 kHz.

The microphones were mounted vertically in two arcs (azimuths $\Psi = 180°$ and $\Psi = 270°$), facing the propeller hub, with the sensing elements 1.2 m away from the propeller hub. The subsequent microphones in both arcs were mounted at polar angles θ of 40°, 20°, 0°, -20°, -40° and -60°, according to the reference frame from Figure 4. Only one microphone arc ($\Psi = 270°$) was used to study the stacked rotors.

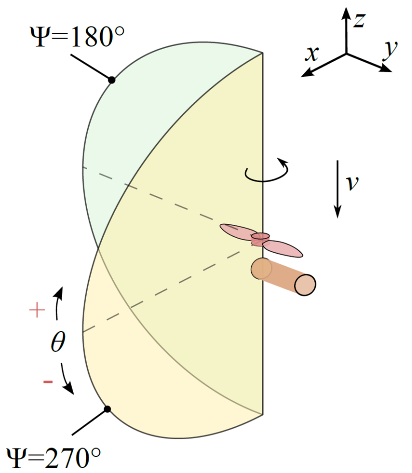

Figure 4: Reference frame used in the research

3.4. Prototypes manufacturing

In this study, rapid prototyping was employed to create prototypes selected for examining the rotor-arm interaction and ducted rotors. All variants of arm geometries were manufactured using 3D printing technology with Fused Deposition Modeling (FDM). 3D printing was also utilized to produce prototypes of rotors and ducts. However, for these components, technologies based on light-curing resin were used: stereolithography (SLA) for the ducts and Digital Light Processing (DLP) for the rotor blades. Resin printing ensured high surface quality of the obtained prototypes. The high quality of geometry reproduction was proven using 3D scans.

4. TEST CASES

4.1. Rotor-arm interaction

The investigation of the rotor-arm interaction involved the use of a commercially available APC 12x5.5 MR propeller in all analyzed configurations. The present study focuses on the scenario where the arm is placed downstream of the propeller at a distance of 15 mm (the axial distance between the trailing edge at the blade tip and the arm surface). The base geometry of the arm was a straight 20 mm diameter tube, as shown in Figure 2. The other cases, designed for noise minimization, are presented in Figure 5.

The concept behind these designs was to limit the surface area exposed to the influence of overpressure fields associated with passing blades, or to reduce the intensity of this interaction by stretching it over time and utilizing beneficial acoustic wave interference. Similar mechanisms are responsible for noise reduction in some turbomachinery applications (Ref. 16) and highly-swept propeller blades (Ref. 17).

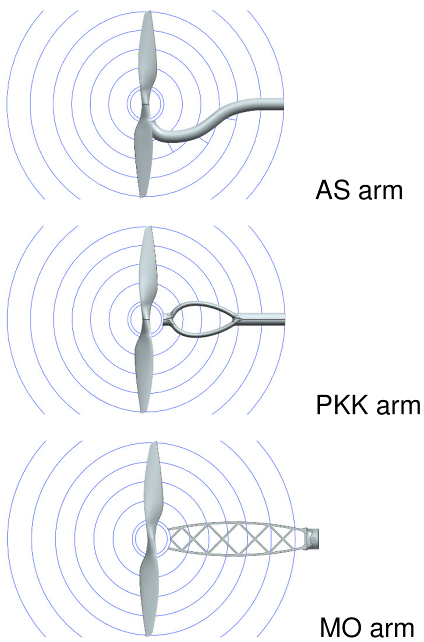

Figure 5: Arm designs for noise minimization

4.2. Stacked rotors

The investigation of stacked rotors involved the use of commercially available propellers with diameters of 10, 11, and 12 inches, and various pitch angles. The research was based on the APC multi-rotor (MR) propeller family.

First, two APC 12x5.5 MR propellers were used to investigate the effect of axial and azimuthal separation between rotors on the achieved performance and noise. Figure 6 shows the adopted symbol convention (rotor azimuthal separation φ is positive if the upper rotor is ahead). Secondly, a number of tests were carried out to find the optimal configuration of rotors in terms of their diameters and pitch values.

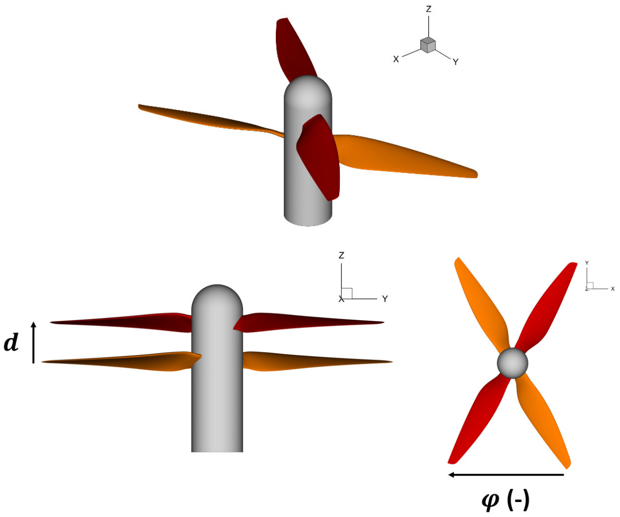

Figure 6: Symbol convention used in stacked rotors research (case shown: $d = 30\ \mathrm{mm}$, $\varphi = -60°$)

4.3. Ducted rotors

In the case of ducted propulsion systems, all components were designed from scratch. The initial design of the rotors and ducts was made using the DFDC program, whose modeling fidelity lies between classical vortex/blade-element methods and a general 3-D vortex-lattice or panel method (Ref. 18). However, due to DFDC's limitations in predicting flow separation at the duct inlet, the final solutions were obtained using RANS-based interactive design aimed at maximization of propulsion efficiency for a given thrust value in hover conditions. An example result of flow simulation for one of the analyzed configurations is presented in Figure 7. No flow separation could be seen at the duct inlet, which is a common issue for ducted rotors operating in hover. To minimize the influence on the weight of the aircraft, it was aimed to develop duct geometries with a chord-to-diameter ratio below 25%. The three duct geometries used in the current study are presented in Figure 8. They were designed to work with the same rotor geometry, designed using DFDC, and have an identical inlet shape. The B6 configuration was the only one with a non-zero diffuser angle at the outlet. All configurations were tested with rotor tip clearance of approximately 0.8 mm.

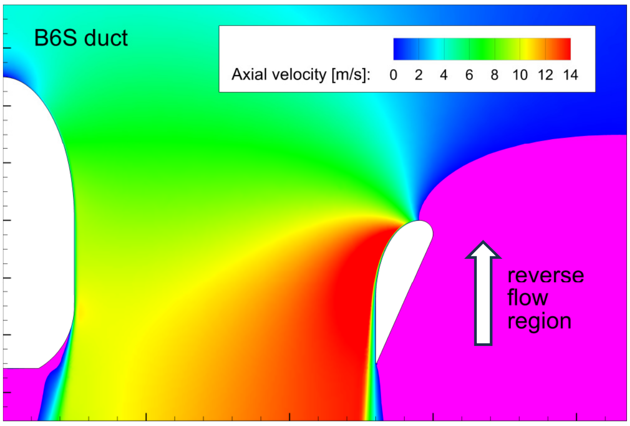

Figure 7: Computed axial velocity contours for the B6S duct with marked reverse flow regions (hover conditions)

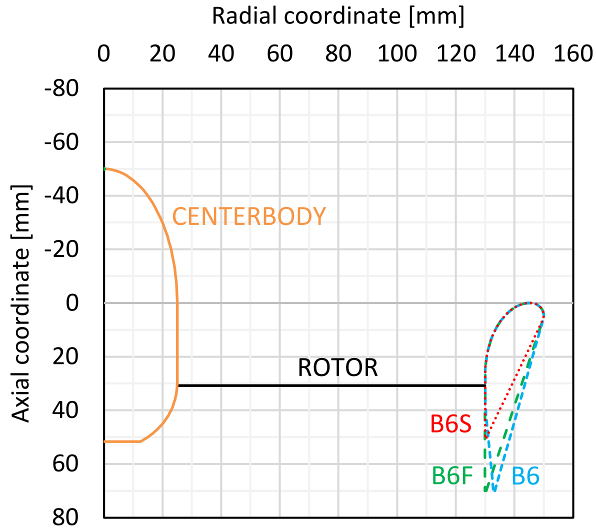

Figure 8: Comparison of the analyzed ducted propulsion configurations

5. RESULTS

5.1. Rotor-arm interaction

Research on the rotor-arm interaction primarily focused on analyzing the impact of various arm geometries on the emitted noise, with their effect on rotor performance being negligible. The noise was measured using two vertical microphone arcs. A-weighted sound pressure levels obtained for the two azimuths are presented in Figure 9 and Figure 10, for arms placed 15 mm downstream of the propeller rotating at 6000 RPM. According to the results of other studies (Ref. 8), the impact of arms on the noise measured in the plane coinciding with the arm axis ($\Psi = 180°$) was significantly smaller than in the plane perpendicular to the arm axis ($\Psi = 270°$).

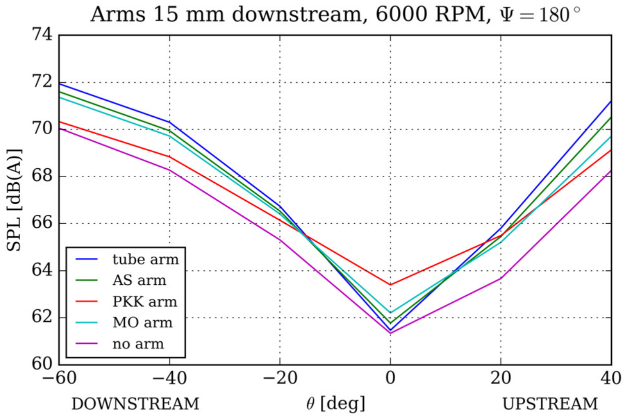

Figure 9 Sound pressure levels measured in the plane coinciding with arm axis (6000 RPM)

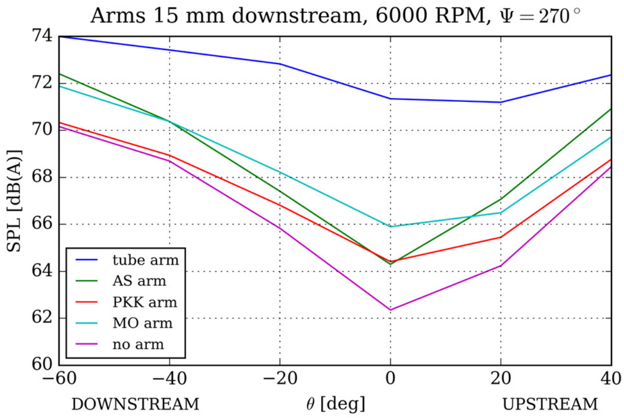

Figure 10 Sound pressure levels measured in the plane perpendicular to the arm axis (6000 RPM)

Due to the abovementioned strong noise directivity, the subsequent discussion focuses on analyzing the results for the azimuth $\Psi = 270°$. Adding an arm in the form of a 20 mm diameter tube (baseline case) 15 mm downstream of the rotor caused an increase in SPL in the range of 4-9 dB(A), depending on the microphone elevation. The proposed concepts of noise-reducing arms (AS, PKK, MO) were capable of significantly reducing the level of emitted noise by up to 7 dB(A) in the propeller rotation plane (Figure 10, $\theta = 0°$). Differences of up to 2 dB(A) can be observed between the proposed arm geometries, depending on the microphone position. It can be seen that for the most downstream and upstream microphone positions, the noise emission for the configuration with the PKK arm approaches the value generated by the isolated rotor (no arm).

The noise spectrum analysis, shown in Figure 11, indicates that the examined interaction primarily contributes to an increase in noise at successive harmonic components of the fundamental blade passing frequency (BPF = 200 Hz). The greatest changes can be observed from the second to approximately the twelfth harmonic – the proposed arm geometries are responsible for reducing noise components within that range.

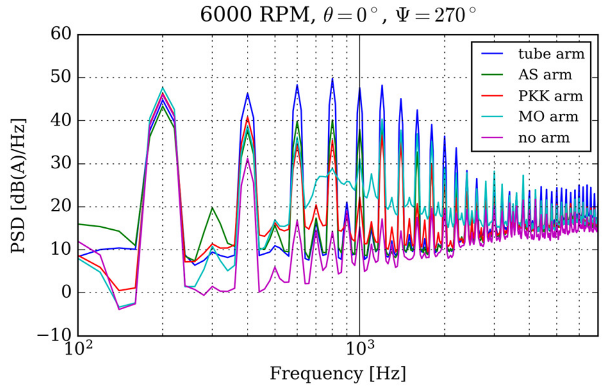

Figure 11 Noise spectra measured in the propeller rotation plane at $\Psi = 270°$

The configuration with the truss MO arm has slightly different noise characteristics than the others. In the frequency range from 700 to 3000 Hz, a clearly greater share of broadband noise can be observed, while the fourth and fifth harmonics of BPF are significantly reduced. The increase in broadband noise in this configuration is an expected effect resulting from the generation of turbulence in the flow through the arm, but is of little significance in relation to the level of tonal components of the noise.

5.2. Stacked rotors

Preliminary stacked rotors research involved testing two APC 12x5.5 MR propellers with a diameter of 12 inches at a rotational speed of 4500 RPM. A series of axial distances between the rotors d and a range of azimuthal separation angles φ were investigated. Figure 12 illustrates the performance results focusing on thrust generation and aerodynamic efficiency (Figure of Merit, FM). It is easy to observe that, in terms of performance, a favorable outcome is associated with a maximized axial separation between the rotors (resulting in increased thrust and efficiency), while the influence of angular separation is slightly smaller but still noticeable. In this case, the optimal configuration appears to be a rotor separation of 50-60 mm and an angular separation of approximately -45°, which indicates the position of the upstream rotor blade behind the blade of the downstream rotor.

In this case, the acoustic analysis focused solely on tonal noise. The sound pressure level of the tonal components $\mathrm{SPL_{tonal}}$ was integrated from 100 Hz to 800 Hz, considering the most important tonal components that were at least 20 dB higher than the broadband noise level. This approach was intended to eliminate the impact of the noise generated by the electric motor on the research conclusions. Figure 13 shows an example of the noise spectrum, with a visible contribution from the motor visible around 1000 Hz and at frequencies above 10000 Hz. The graph also shows the tonal noise components used to calculate the $\mathrm{SPL_{tonal}}$ value for the case presented. A significant level of broadband noise can be observed in the range of 3000-10000 Hz, especially when analyzing A-weighted spectra. However, the tonal components of noise generated by drones are considered the main cause of their high nuisance to humans (Ref. 3). This is another reason why the current analysis is limited to tonal noise only.

The results from noise measurements in the plane of the upstream rotor are presented in Figure 14. Analysis of the data indicates that the configuration optimal for aerodynamic performance is characterized by an average level of emitted noise. In this case, a strong trend is evident, correlating the increase in $\mathrm{SPL_{tonal}}$ with the reduction of angular separation between the rotors. The quietest variant is observed with propellers set at an angle of approximately 90° relative to each other, regardless of the axial separation distance d. This is the effect of a favorable 90-degree phase shift between the acoustic signals generated by each propeller, causing destructive interference of acoustic waves.

In comparison to a single APC 12x5.5 MR propeller tested at the same rotational speed of 4500 RPM (first row in Table 1), the configuration of stacked rotors with a separation of $d = 60\ \mathrm{mm}$ and $\phi = 90°$ resulted in a thrust increase of 53%, with an FM increase of 7.3%, and a tonal noise reduction of 7.5 dB(A). Conducting a similar comparison while maintaining the same thrust value (with an increase in the rotational speed of the single propeller to approximately 5500 RPM), stacked rotors enable a 5.1% increase in FM, and a tonal noise reduction of 15.4 dB(A). This demonstrates the significant potential of stacked rotors configurations. Similar trends in noise and performance characteristics were observed in a numerical investigation performed using the Vortex Particle Method, and presented in Ref. 19.

The potential of stacked rotors could be even greater, especially if further optimization of rotor diameters and blade geometries is considered. In the presented research, a variety of APC MR propellers were tested in various stacked configurations to further investigate aeroacoustic performance improvement possibilities. All cases were tested at three rotational speeds – 4000, 4500, and 5000 RPM – with an axial separation between rotors of $d = 60\ \mathrm{mm}$ and an azimuthal separation of $\phi = 90°$. The results for 4500 RPM and cases interpolated to obtain 8 N of thrust are summarized in Table 1. Interpolating the results was crucial from the perspective of acoustic comparisons due to the strong correlation of noise and thrust values.

The analysis of the collected experimental data demonstrated that the use of two identical propellers (12x5.5) constitutes one of the best solutions in terms of both efficiency (FM) and generated noise. The only quieter configuration involved using a upstream propeller with a smaller pitch (12x4.5), which allowed for a further noise reduction of 2.3 dB(A). A configuration enabling a slight improvement in efficiency (by 0.8%) was the variant with a smaller upstream propeller but maintaining the same pitch (11x5.5). In this case, however, the performance improvement resulted in a slight increase in noise by 0.9 dB(A) compared to two identical propellers. Other configurations, with the upstream propeller of a larger diameter and/or greater pitch, resulted in a deterioration of efficiency and an increase in noise levels. This is consistent with expectations, as the downstream propeller operates in a forced flow (higher axial flow velocity) and increasing its pitch has a theoretical justification. Ultimately, the quietest of the examined configurations (12x4.5 + 12x5.5) was found to be 17.2 dB(A) quieter and 5% more efficient than a single 12x5.5 propeller, while maintaining the same level of generated thrust.

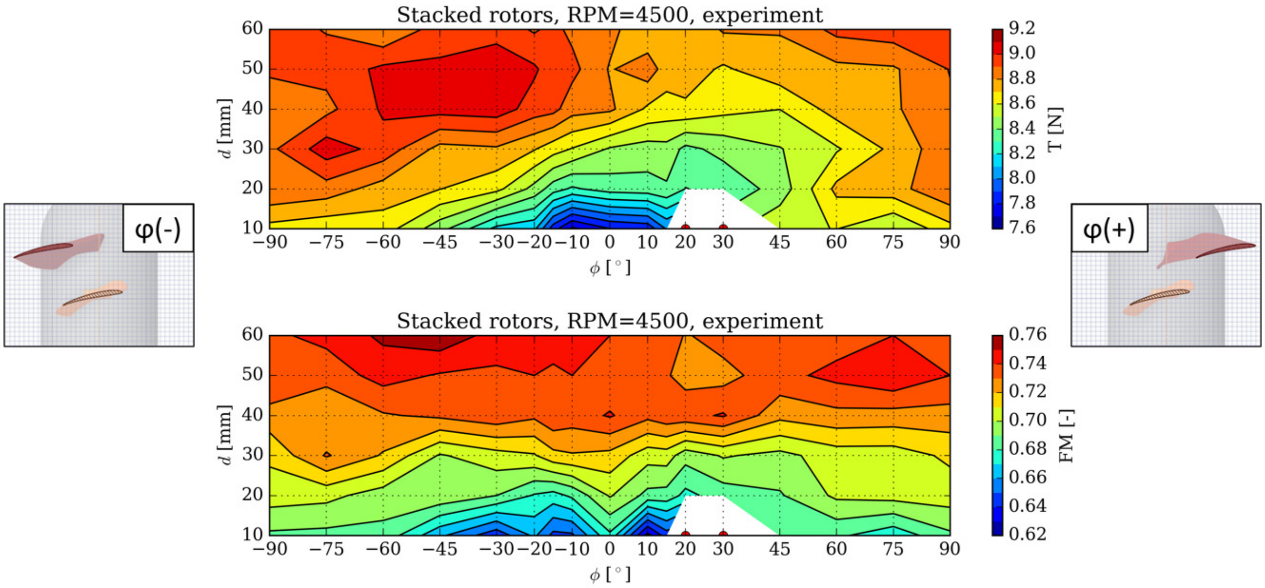

Figure 12: Measured thrust and Figure of Merit (FM) characteristics for the configuration of two stacked APC 12x5.5 MR propellers

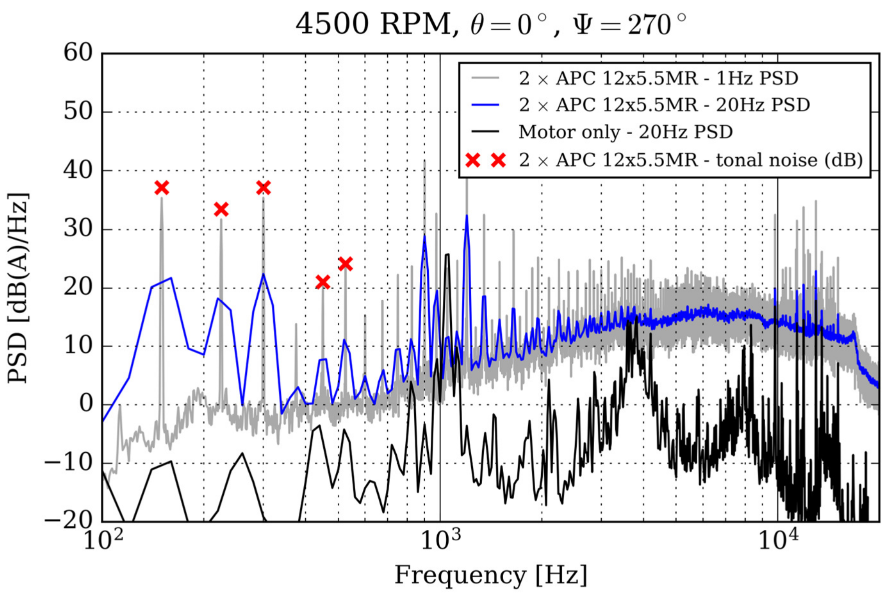

Figure 13: Sound spectra for two stacked APC 12x5.5 MR propellers and isolated motor noise, with marked tonal noise components used to calculate $\mathrm{SPL_{tonal}}$ for the case presented

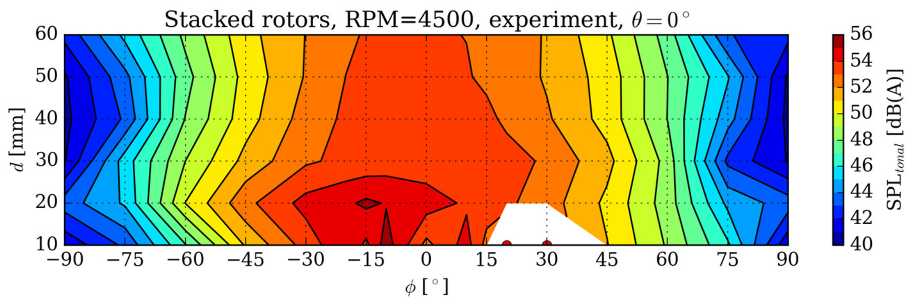

Figure 14: Measured noise ($\mathrm{SPL_{tonal}}$) characteristics for the configuration of two stacked APC 12x5.5 MR propellers

Table 1: Summary of tests on stacked rotors with different diameters and pitch angles ($d = 60$ mm and $\phi = 90°$, noise measurement at $\theta = 0°$)

Upstream rotor (APC MR)	Downstream rotor (APC MR)	4500 RPM			T = 8 N (interpolated)	
		T [N]	FM [-]	SPL_{tonal} [dB(A)]	FM [-]	SPL_{tonal} [dB(A)]
12x5.5	-	5.76	0.671	48.7	0.681	54.7
12x5.5	12x5.5	8.79	0.720	41.2	0.715	39.8
12x5.5	12x4.5	7.51	0.681	44.4	0.682	45.4
12x4.5	12x5.5	8.12	0.716	37.9	0.715	37.5
12x5.5	11x5.5	7.59	0.688	44.0	0.692	44.8
11x5.5	12x5.5	8.02	0.721	40.7	0.721	40.7
12x5.5	10x5.5	6.90	0.649	45.4	0.657	48.3
10x5.5	12x5.5	7.39	0.706	46.2	0.693	45.7
11x4.5	12x5.5	7.57	0.713	39.9	0.715	41.0
10x4.5	12x5.5	7.05	0.702	43.9	0.710	45.5

5.3. Ducted rotors

Three variants of ducted propulsors, described in section 4.3, were examined over a range of rotational speeds: 3000, 4000, 5000, and 6000 RPM. As in the previous case, the obtained results were compared with those for the isolated APC 12x5.5 MR propeller, which has a diameter similar to that of the ducts (12 in vs 30 cm). The characteristics of thrust and Figure of Merit (calculated based on the outer duct radius) are presented in Figure 15 and Figure 16, respectively. It can be seen that all analyzed ducted configurations have similar thrust curves and produce 14% to 18% more thrust than the isolated APC 12x5.5 MR propeller, depending on the RPM value. From a performance perspective, the gains from using ducted rotors are even higher, offering the possibility of increasing hover efficiency (FM) by up to 24% (at 12 N of thrust). This is due to the significant amount of thrust generated by the duct inlet. For the presented cases, the contribution of the ducts to the generated thrust ranges from 41.8% to 48.5%, as shown in Figure 17. A high correlation can be seen between FM and T_D/T characteristics. The most efficient configuration is the B6, equipped with a diffuser and a duct chord length of 70 mm. B6F turned out to be slightly worse due to the lack of a diffuser. The shortest of the analyzed ducts, B6S, with a chord length reduced to 50 mm, had the lowest efficiency among these three cases, but still significantly higher than the isolated APC 12x5.5 MR propeller.

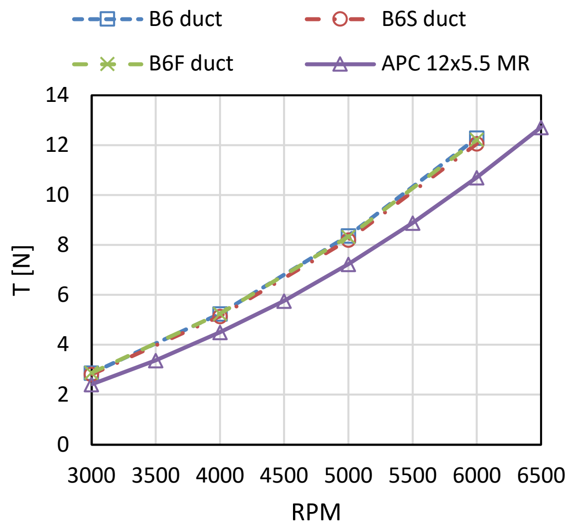

Figure 15: Thrust characteristics of analyzed ducted propulsors and isolated APC 12x5.5 MR propeller

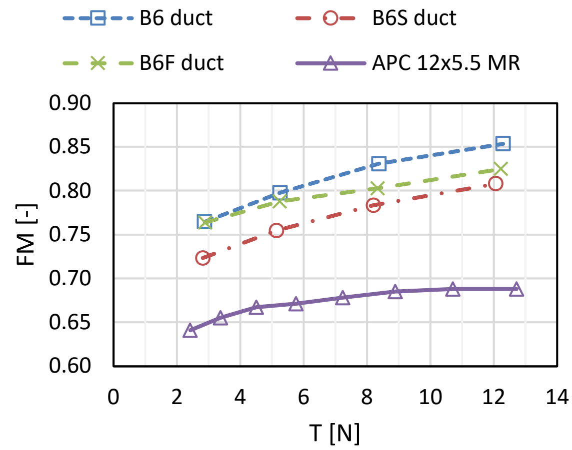

Figure 16: Figure of Merit characteristics of analyzed ducted propulsors and isolated APC 12x5.5 MR propeller

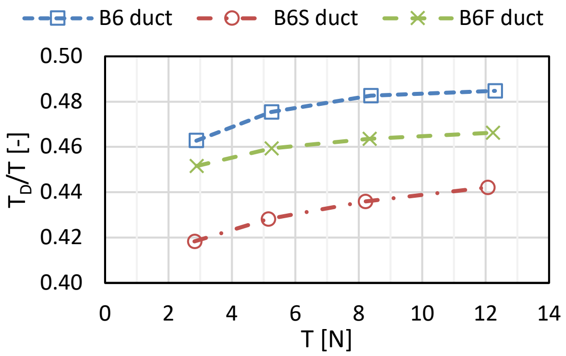

Figure 17: The share of duct in the total thrust generated by the ducted propulsors

Prior to conducting the noise analysis of the ducted propulsors, a validation of the accuracy of the acoustic measurements was performed. Given the noise caused by the vibrations of the electric motor, which was already evident in the case of stacked rotors tests, there was a risk that the additional rigid structure required to mount the ducts would increase the contribution of mechanical noise. To verify this hypothesis, tests were conducted on the isolated propeller both in the presence of the new structure and without it. The measured noise spectra are presented in Figure 18. Significant changes in the measured noise levels are visible across a wide range of frequencies, mainly in the tonal noise components. Only the peak at the blade passing frequency (BPF) was recorded at nearly the same level. Eliminating the influence of the additional structure on the measured noise spectrum would require the use of an additional vibration-absorbing element between the electric motor and the frame, which is being considered for the future. For now, however, it was decided to focus solely on the analysis of tonal noise at the BPF ($\mathrm{SPL_{BPF}}$), as it is the main component of the noise.

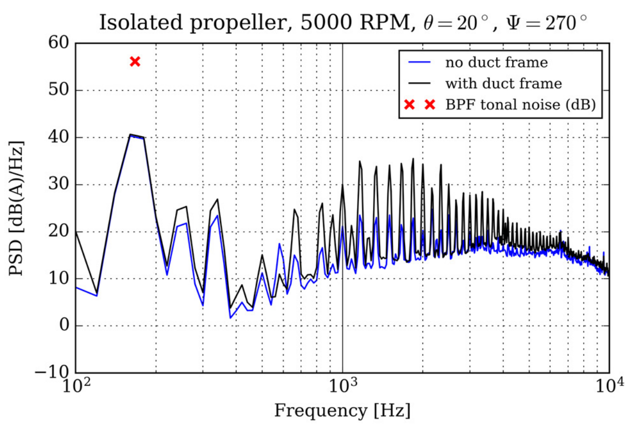

Figure 18: Influence of duct frame on noise spectra of isolated propeller

A comparison of the $\mathrm{SPL_{BPF}}$ noise for the three tested ducted configurations and the isolated propeller is presented in Figure 19. In this case, the results are shown for the microphone placed downstream of the rotor ($\theta = -40°$) - the microphone positioned in the plane of blade rotation was affected by additional noise shielding effects by the test stand frame. According to Figure 19, all ducted drive configurations provide a similar noise reduction for thrust values above 8 N. For lower thrust values, the B6S configuration, equipped with shorter duct chord length, proved to be slightly less effective in noise reduction. One of the potential reasons for this could be the change in the way acoustic waves interfere depending on the rotor's rotational speed and the duct geometry.

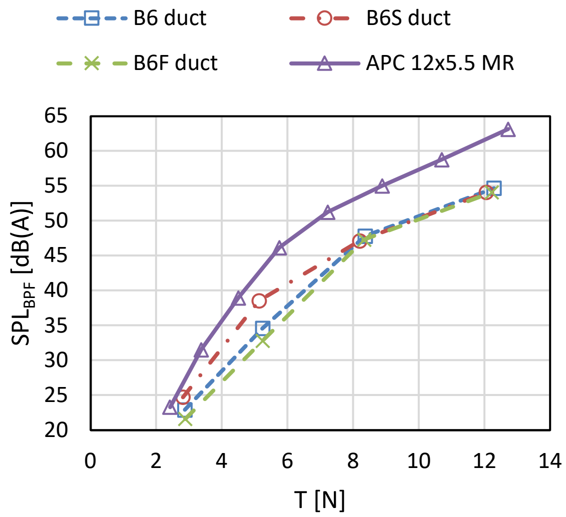

Figure 19: Comparison of tonal noise at the blade passing frequency for ducted rotors and the isolated propeller ($\Psi = 180°$, $\theta = -40°$)

However, comparing ducted rotors and the isolated propeller under the assumption of the same required thrust value favors the former. The use of a ducted propulsor typically involves an increase in the weight of the aircraft, which must be compensated for by increasing the thrust. Therefore, an additional analysis was conducted including the need to increase the thrust for the ducted configurations by 12.5% to 25%, corresponding to the assumed weight of the duct ranging from 100 to 200 grams. The results of the comparison are presented in Table 2. In this analysis, mechanical power was used as the dimensional quantity to assess the performance. It can be seen that for the same thrust (8 N), all ducted configurations are both more efficient (as indicated by the higher FM value in Figure 16) and quieter than the isolated APC 12x5.5 MR propeller. However, when assuming 9 N of required thrust for ducted propulsors, they have a similar power requirement to the isolated propeller but with $\mathrm{SPL_{BPF}}$ reduced by about 4.6 dB(A). Increasing thrust further, up to 10 N, results in at least 15.7% higher power demand with a noise reduction of about 2.8 dB(A) compared to the APC 12x5.5 MR propeller. This proves that, at a given scale, ducted propulsors are a good solution for noise reduction but need to be lightweight to maintain a similar performance level to traditional propellers.

Table 2 Comparison of the performance and noise of the APC 12x5.5 MR propeller and ducted configurations (noise measurement at $\theta = -40°$)

Configuration	T = 8 N (interpolated)		T = 9 N (interpolated)		T = 10 N (interpolated)	
	P [W]	$\mathrm{SPL_{BPF}}$ [dB(A)]	P [W]	$\mathrm{SPL_{BPF}}$ [dB(A)]	P [W]	$\mathrm{SPL_{BPF}}$ [dB(A)]
APC 12x5.5 MR	79.4	53.5	-	-	-	-
B6 duct	67.0	46.2	79.1	48.9	91.9	50.7
B6F duct	69.0	45.7	81.7	48.5	95.0	50.2
B6S duct	70.8	46.6	83.6	48.6	97.1	50.4

6. CONCLUSIONS

Unconventional low-noise propulsion designs for UAV/UAM applications were proposed and verified in terms of aeroacoustic performance through an experimental test campaign performed in the anechoic chamber of the Lukasiewicz – Institute of Aviation. The research involved investigations in three areas: the rotor-arm interaction, stacked rotors and ducted propulsors.

The most important conclusions of the work are:

1. The rotor-arm aeroacoustic interaction can significantly affect the noise signature of the propulsion system. The measured noise emission (SPL) of a propeller increased by up to 9 dB(A) when a tube arm was placed 15 mm downstream of the propeller. Using the proposed arm designs reduced noise emission by up to 7 dB(A), resulting in only a slight increase in noise compared to the isolated propeller.
2. Stacked rotors proved to be a very promising way of increasing propulsion performance (thrust and efficiency) and reducing noise emissions without increasing the propulsor diameter. The best overall analyzed configuration consisted of two APC MR propellers (12x4.5 and 12x5.5) with an azimuthal separation of 90° and an axial separation of 60 mm. In this case, the obtained noise reduction reached 17.2 dB(A) compared to the isolated APC 12x5.5 MR propeller, while aerodynamic efficiency improved by 5%.
3. Ducted propulsion, with a low chord-to-diameter ratio below 25%, seemed to be another interesting option for improving UAV/UAM propulsion characteristics without changing size restrictions. However, its efficiency improvement and noise reduction potential were somewhat limited due to the need to achieve a higher thrust to compensate for the increased weight of the propulsion system. Nevertheless, in the most realistic scenario of a 12.5% necessary thrust increase, the analyzed ducted configurations allowed for a noise reduction of about 4.6 dB(A) without increasing the power demand compared to the isolated APC 12x5.5 MR propeller.

One of the more interesting aspects would be to test all the presented concepts simultaneously in one integrated propulsion system demonstrator. This type of research is planned to be carried out in the near future.

Author contact:

Adam Sieradzki
adam.sieradzki@ilot.lukasiewicz.gov.pl

Pawel Kekus-Kumor
pawel.kekus-kumor@ilot.lukasiewicz.gov.pl

Witold Klimczyk
witold.klimczyk@ilot.lukasiewicz.gov.pl

7. ACKNOWLEDGMENTS

Computations were carried out using the computers of the Centre of Informatics Tricity Academic Supercomputer & Network.

8. REFERENCES

[1] S. A. Rizzi *et al.*, 'Urban Air Mobility Noise: Current Practice, Gaps, and Recommendations', NASA, Washington, DC, USA, Oct. 2020.

[2] O. Barbara, L. Seth, A. Roalt, D. Schreckenberg, and M. V. Miltenburg, 'Association Between Short-Term Annoyance and Several Physiological Parameters During Different Amounts of Nocturnal Aircraft Noise Exposure', *Transactions on Aerospace Research*, vol. 2020, no. 4, pp. 1–12, Dec. 2020, doi: 10.2478/tar-2020-0018.

[3] A. W. Christian and R. Cabell, 'Initial Investigation into the Psychoacoustic Properties of Small Unmanned Aerial System Noise', in *23rd AIAA/CEAS Aeroacoustics Conference*, in AIAA AVIATION Forum. , American Institute of Aeronautics and Astronautics, 2017. doi: 10.2514/6.2017-4051.

[4] R. Serré, H. Fournier, and J.-M. Moschetta, 'A design methodology for quiet and long endurance MAV rotors', *International Journal of Micro Air Vehicles*, vol. 11, Jan. 2019, doi: 10.1177/1756829319845937.

[5] O. Gur, J. Silver, R. Dítě, and R. Sundhar, 'Optimized Performance and Acoustic Design for Hover-Propeller', in *AIAA AVIATION 2021 FORUM*, Virtual Event: American Institute of Aeronautics and Astronautics, Aug. 2021. doi: 10.2514/6.2021-2222.

[6] D. Ingraham, J. S. Gray, and L. V. Lopes, 'Gradient-Based Propeller Optimization with Acoustic Constraints', in *AIAA Scitech 2019 Forum*, San Diego, California: American Institute of Aeronautics and Astronautics, Jan. 2019. doi: 10.2514/6.2019-1219.

[7] W. Klimczyk and A. Sieradzki, 'RANS-Based Aeroacoustic Global Sensitivity Study and Optimization of UAV Propellers', *Aerospace*, vol. 10, no. 3, Art. no. 3, Mar. 2023, doi: 10.3390/aerospace10030306.

[8] N. S. Zawodny and D. D. Boyd, 'Investigation of Rotor–Airframe Interaction Noise Associated with Small-Scale Rotary-Wing Unmanned Aircraft Systems', *Journal of the American Helicopter Society*, vol. 65, no. 1, pp. 1–17, Jan. 2020, doi: 10.4050/JAHS.65.012007.

[9] P. Martin and C. Tung, 'Performance and Flowfield Measurements on a 10-inch Ducted Rotor VTOL UAV', presented at the Vertical Flight Society Annual Forum & Technology Display - Forum, The Vertical Flight Society, 2004.

[10] J. L. Pereira, 'Hover and Wind-Tunnel Testing of Shrouded Rotors for Improved Micro Air Vehicle Design', Aug. 2008, Accessed: Mar. 15, 2023.

[11] R. Goudswaard, 'Aerodynamic performance of a small-scale ducted rotor in hover: An experimental study on the effect of the tip gap', 2021.

[12] T. Zhang and G. N. Barakos, 'High-fidelity numerical analysis and optimisation of ducted propeller aerodynamics and acoustics', *Aerospace Science and Technology*, vol. 113, p. 106708, Jun. 2021, doi: 10.1016/j.ast.2021.106708.

[13] A. Sieradzki, P. Kekus, and W. Klimczyk, 'Validation of a Surrogate-Based Methodology for Low-Noise UAV/UAM Rotor Design', in *49th European Rotorcraft Forum 2023*, Bückeburg, Germany, Sept. 2023.

[14] P. Kekus-Kumor, A. Sieradzki, 'Experimental investigation of unmanned air vehicle rotor aeroacoustics using benchmark geometries', in *52nd International Congress and Exposition on Noise Control Engineering*, Chiba, Japan, Aug. 2023, doi: 10.3397/IN_2023_0769.

[15] D. Weitsman, J. H. Stephenson, and N. S. Zawodny, 'Effects of flow recirculation on acoustic and dynamic measurements of rotary-wing systems operating in closed anechoic chambers', *The Journal of the Acoustical Society of America*, vol. 148, no. 3, pp. 1325–1336, Sep. 2020, doi: 10.1121/10.0001901.

[16] E. Envia and M. Nallasamy, 'Design Selection and Analysis of a Swept and Leaned Stator Concept', *Journal of Sound and Vibration*, vol. 228, no. 4, pp. 793–836, Dec. 1999, doi: 10.1006/jsvi.1999.2441.

[17] R. J. Klatte and F. B. Metzger, *Influence of Noise Reduction on Weight and Cost of General Aviation Propellers*. Windsorr Locks, Conn.: Hamilton Standard Division of United Technologies Corp., 1979.

[18] M. Drela and H. Youngren, 'Axisymmetric Analysis and Design of Ducted Rotors'. Massachusetts Institute of Technology, 2005.

[19] W. Klimczyk, P. Kekus-Kumor, and A. Sieradzki, 'Experimental Validation of Vortex Particle Method for Modeling of Rotor Interaction Noise', in *30th AIAA/CEAS Aeroacoustics Conference (2024)*, Rome, Italy, Jun. 2024.

9. CLASSIFICATION & COPYRIGHT

The paper must be unclassified for release to the public and cleared by the appropriate company and/or government agency if necessary. CEAS and its national member societies shall be allowed to publish the paper. The copyright information is stated on the Forum website https://www.rotorcraft-forum.eu/ and on the front page of this template. All papers presented at the ERF will be published as ERF proceedings. In addition they will be available in a freely accessible web-based repository 2 years after the respective conference.